Processing and Application of Ceramics 11 [1] (2017) 45–51
DOI: 10.2298/PAC1701045N

BY-NC-ND

Structural, optical and electrical properties of reactively sputtered Cr_xN_y films: Nitrogen influence on the phase formation

Mirjana Novaković*, Maja Popović, Zlatko Rakočević, Nataša Bibić

University of Belgrade, VINČA Institute of Nuclear Sciences, 11001 Belgrade, Serbia

Received 12 December 2016; Received in revised form 1 February 2017; Accepted 25 February 2017

Abstract

The properties of various Cr_xN_y films grown by direct current (DC) reactive sputtering process with different values of nitrogen partial pressures (0, 2×10^{-4}, 3.5×10^{-4} and 5×10^{-4} mbar) were studied. The structural analysis of the samples was performed by using X-ray diffraction and transmission electron microscopy (TEM), while an elemental analysis was realized by means of Rutherford backscattering spectrometry. By varying nitrogen partial pressure the pure Cr layer, mixture of Cr, Cr_2N and CrN phases, or single-phase CrN was produced. TEM analysis showed that at $p_{N_2} = 2\times10^{-4}$ mbar the layer has dense microstructure. On the other hand, the layer deposited at the highest nitrogen partial pressure exhibits pronounced columnar structure. The optical properties of Cr_xN_y films were evaluated from spectroscopic ellipsometry data by the Drude or combined Drude and Tauc-Lorentz model. It was found that both refractive index and extinction coefficient are strongly dependent on the dominant phase formation (Cr, Cr_2N, CrN) during the deposition process. Finally, the electrical studies indicated the metallic character of Cr_2N phase and semiconducting behaviour of CrN.

Keywords: *chromium nitrides, spectroscopic ellipsometry, electrical properties, microstructure, thin films*

I. Introduction

Transition metal nitrides exhibit highly covalent bonds in simple, usually cubic structures, which give them an extreme hardness, high corrosion and oxidation resistance and excellent mechanical and high-temperature stability [1–4]. Due to their excellent tribological characteristics, they have become important materials for cutting tools and wear applications, as diffusion barriers in microelectronics, and as corrosion and abrasion-resistant coatings on optical and mechanical components [5]. TiN and CrN are the most extensively investigated hard coatings. Besides its good mechanical properties TiN is not always corrosion resistant due to the presence of micro defects in the layers, while dense microstructure of CrN provide high wear and corrosion resistance [6]. Much research is being conducted to study growth and properties of CrN film deposited by CVD and PVD methods [7]. Nevertheless PVD methods, such as unbalanced magnetron sputtering, metal vapour vacuum arc, RF reactive sputtering, pulsed DC magnetron sputtering, arc discharge etc., are quite common for the deposition of CrN films, whereas CVD methods are not as popular.

In physical vapour deposition chromium-nitride films can grow in form of cubic CrN or hexagonal Cr_2N phases, with Cr_2N phase exhibiting a higher hardness. On the other hand, the CrN phase is also interesting due to its magnetic, optical and electronic properties, in the recent studies being reported as a semiconductor material [8,9]. For sputtered thin films, process parameters such as gas partial pressure, bias voltage, temperature, and growth rate strongly influence the film properties. By controlling the partial pressure of nitrogen during reactive sputtering it is possible to produce films ranging in composition from the pure Cr through Cr_2N-CrN mixtures to pure CrN as the amount of nitrogen is increased [10]. The composition and growth parameters influence the microstructure, optical and electrical properties of the resulting materials. Although the microstructural features of CrN and Cr_2N have been studied previously [10–12] low attention was given to their optical properties and electronic structure and their correlation to the process parameters during the deposition.

* Corresponding author: tel/fax: +381 11 630 8425,
e-mail: *mnovakov@vinca.rs*

In this work the microstructure, optical and electrical properties of various Cr_xN_y coatings were studied. We investigate the effect of the nitrogen partial pressure on the phase formation (Cr, Cr_2N, CrN) and, subsequently, on the properties of the produced coatings. Chemical composition of the layers was identified by Rutherford backscattering spectrometry (RBS), while X-ray diffraction (XRD) and transmission electron microscopy (TEM) were used for the structural characterization and the phase identification. The optical properties were determined by spectroscopic ellipsometry (SE), SE data being analysed with the Bruggeman Effective Medium Theory (BEMT) [13]. We showed that spectroscopic ellipsometry can be used as an alternative technique for phase identification of single-phases (Cr, Cr_2N and CrN) and their volume fractions in the layers. Using the Drude and combined Drude-Tauc Lorentz model [13–15], we defined the optical constants (refractive index n and extinction coefficient k) of the layers. We found that both optical and electrical properties of Cr_xN_y layers are strongly determined by the growing phase.

II. Experimental

Cr_xN_y films used in the present experiments were deposited by means of DC reactive ion sputtering in a Balzers Sputtron II system. The layers were grown on commercial Si(100) wafers. The substrates were cleaned by standard HF etching and dip in deionized water before being mounted into the deposition chamber. Then, they were ion etched for 2 minutes in Ar atmosphere at a pressure of 1×10^{-3} mbar and a negative bias voltage of 1 kV applied to the substrate holder. The base pressure prior to sputtering was approximately 5×10^{-6} mbar. Sputter deposition was performed using a Cr target (99.9%) in a mixed Ar (99.999%) and N_2 (99.999%) discharge. During deposition, the argon partial pressure was initially set to 1×10^{-3} mbar and the reactive gas, i.e. N_2, was subsequently added to obtain the desired gas composition. The nitrogen partial pressure was set either to 2×10^{-4}, 3.5×10^{-4}, or 5×10^{-4} mbar. The layers were grown at room temperature (RT), at a rate of ~10 nm/min, to a total thickness of 240–280 nm. The pure Cr film (p_{N_2} = 0 mbar), with the thickness of ~220 nm was also deposited. The thicknesses of the deposited structures were measured with a profilometer and confirmed by TEM.

For RBS (Rutherford backscattering spectrometry) analysis we used a 900 keV He^{2+} ion beam, generated by the IONAS facility in Göttingen [16]. We collected random RBS spectra at normal incidence to the sample surface with two detectors, positioned at 165° scattering angle in ibm geometry. The experimental spectra were fitted by using the Data Furnace code [17]. Transmission electron microscopy was done on a Philips EM 400T microscope operated at 120 keV, the samples being prepared for cross-sectional analysis by standard technique of ion beam thinning. Bright-field contrast imaging was done, and we also used micro-diffraction (MD) analysis to study the crystalline structure of the samples. XRD measurements were carried out at normal and grazing incidence on a standard Bruker D8 Diffractometer with parallel beam optics using Cu K_α diffraction patterns. Angle 2θ was scanned in the range from 30° to 70° with step of 0.02°, in time sequence of 10 s.

SE data were obtained using HORIBA-Jobin Yvon variable angle spectroscopic ellipsometer (model UVISEL 5) equipped with DeltaPsi 2 data analysis software [18]. The ellipsometer consisted of a light source, a monochromator, a photoelastic modulator, collimating optics, polarizing elements, a sample holder, and a detector. Simultaneously, the system acquired a spectrum ranging from 0.6 to 4.8 eV with 0.1 eV intervals. Acquisition time per each point was 200 ms. SE measurements were taken using 1 mm spot size and at an angle of incidence of 70°. We also measured sheet resistance of the samples with a four point probe, the values being calculated in specific resistivity to compare the results.

III. Results and discussion

3.1. Composition and microstructure

In general, elemental composition measurements carried out by RBS on chromium-nitride samples revealed homogeneous Cr and N concentrations over the whole depth of the layers, which was shown in our previous paper [19]. For illustration, the Cr concentration profiles in Cr_xN_y layers, as deduced by means of the WiNDF code from the experimental RBS spectra were presented in Fig. 1. The layers have different thickness, but we can see uniform Cr depth profiles. The presented spectra clearly show that the nitrogen partial pressure determines the composition of the deposited layers, which is manifested in the decrease of the Cr concentration with the increase of the N_2 partial pressure. More precise insight into the layers composition can be revealed

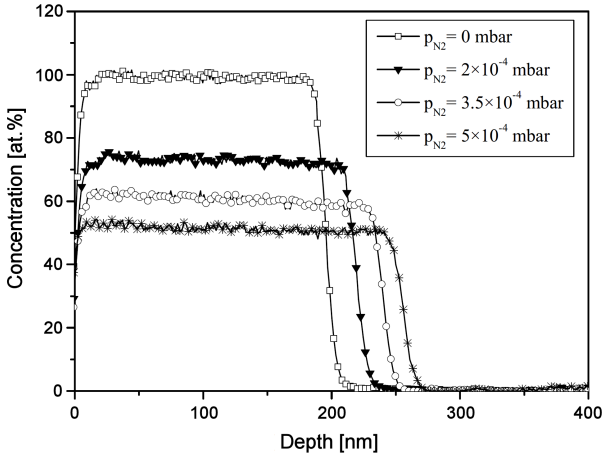

Figure 1. Cr depth profiles in Cr_xN_y films deposited at different nitrogen partial pressures (0, 2×10^{-4}, 3.5×10^{-4} and 5×10^{-4} mbar)

Table 1. Chromium nitride thin film compositions obtained from RBS analyses (the films were deposited under the different values of nitrogen partial pressure, p_{N_2})

Sample	S-1	S-2	S-3	S-4
p_{N_2} [mbar]	0	2×10^{-4}	3.5×10^{-4}	5×10^{-4}
Cr [at.%]	100	73	61	51
N [at.%]	0	27	39	49

by observing the extracted Cr/N ratios for the deposited layers, presented in Table 1. Sample S-1 corresponds to the pure Cr coating, having 100 at.% of chromium, since it was deposited with no flow of nitrogen in the chamber. The extracted Cr/N ratios for the lower nitrogen partial pressures of 2×10^{-4} mbar and 3.5×10^{-4} mbar, clearly showed that the metal-to-nitrogen ratio is ~73/27 and ~61/39, respectively, hinting the formation of nonstoichiometric Cr_2N phase. The sample S-4 deposited at the highest nitrogen pressure (5×10^{-4} mbar) lead to near stoichiometric composition of Cr/N, with the mean atomic composition of $Cr_{51}N_{49}$. This is an indication that under these conditions the pure CrN phase is formed.

Figure 2 shows XRD spectra taken from the samples S-2 and S-3, deposited at nitrogen partial pressure of 2×10^{-4} and 3.5×10^{-4} mbar, respectively. These data indicate that different phases are present in the layers. At low nitrogen partial pressure of 2×10^{-4} mbar the film S-2 contains a mixture of Cr, Cr_2N and CrN phases. When the nitrogen partial pressure is increased to 3.5×10^{-4} mbar (the sample S-3) again the mixture of Cr + Cr_2N + CrN was formed, with larger amount of Cr_2N phase, which is visible through the appearance of new peaks at around 68°. In both spectra the peaks are overlapped due to their large width, indicating very fine-grained structure of the layers. Figure 3 shows XRD spectrum corresponding to the sample S-4 deposited at 5×10^{-4} mbar of nitrogen. Well defined diffraction pattern of the pure fcc CrN phase was obtained, with strong (111) preferred orientation and weaker peaks

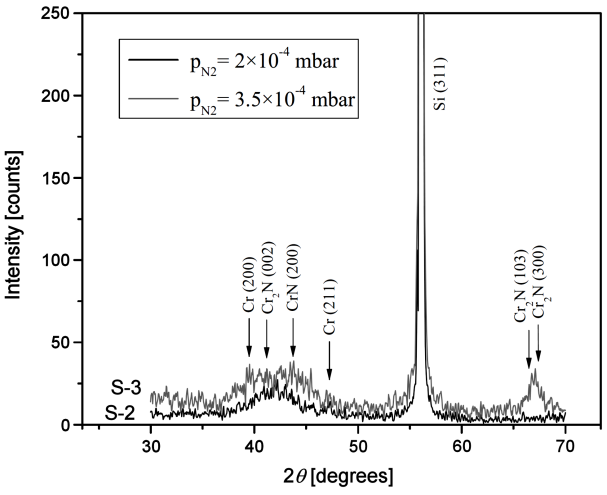

Figure 2. XRD spectra of Cr_xN_y layers deposited at nitrogen partial pressure of: 2×10^{-4} mbar (S-2, black line) and 3.5×10^{-4} mbar (S-3, grey line)

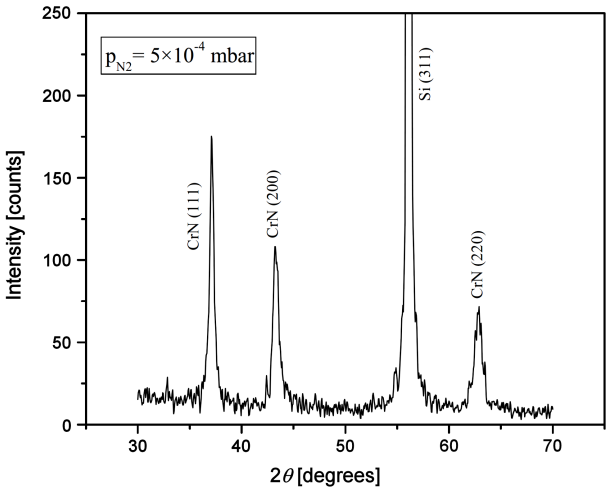

Figure 3. XRD pattern of CrN coating deposited at nitrogen partial pressure of 5×10^{-4} mbar

along (200) and (220) planes, in accordance with minimization of the overall energy of the film. This result is in good agreement with Lu *et al.* [20] who found that the deposited CrN films exhibit a (111) texture. The XRD reflections of CrN film are shifted to lower angular values than expected, which is typical for in-plane compressed d-metal nitrides [13,14]. The deduced lattice parameter of 0.4183 nm found to be in the range of the values characteristic for polycrystalline CrN films: a_0 = 0.4133–0.4185 nm [3,21]. The average grain size of the CrN films, estimated from the FWHM of the XRD lines using the Scherrer's formula, was found to be 14 ± 2 nm.

Figure 4 shows typical cross-section TEM images of Cr_xN_y thin films deposited under different nitrogen partial pressures. One sees that nitrogen pressure during deposition have significant influence on the microstructure of the layers. Bright-field image of the S-2 layer deposited at the lowest nitrogen partial pressure of 2×10^{-4} mbar exhibit a dense morphology, as shown in Fig. 4a. With increasing p_{N_2} to 3.5×10^{-4} mbar (Fig. 4b) the microstructure is less compact with an indication of columnar growth. Diffraction rings on the corresponding MD patterns for both low-nitrogen-pressure layers are blurred and reveal no obvious phases. This is the consequence of two effects: i) the presence of more than one phase and ii) the formation of very small crystalline grains. This is supported by interpretation of corresponding XRD spectra, which showed fine-grained mixture of Cr, Cr_2N and CrN phases. When the nitrogen partial pressure was increased to 5×10^{-4} mbar (Fig. 4c) a pronounced columnar structure of the layer is obvious. Columnar growth is present throughout the whole film thickness, with the columns width of few tens of nanometers. The corresponding MD pattern reveals obvious CrN phase. The first three rings belong to (111), (200) and (220) CrN phase, while the outer rings correspond to higher indexed planes of this phase. The changes in the morphology of the growing film during deposition were investigated by Hones *et al.* [22]

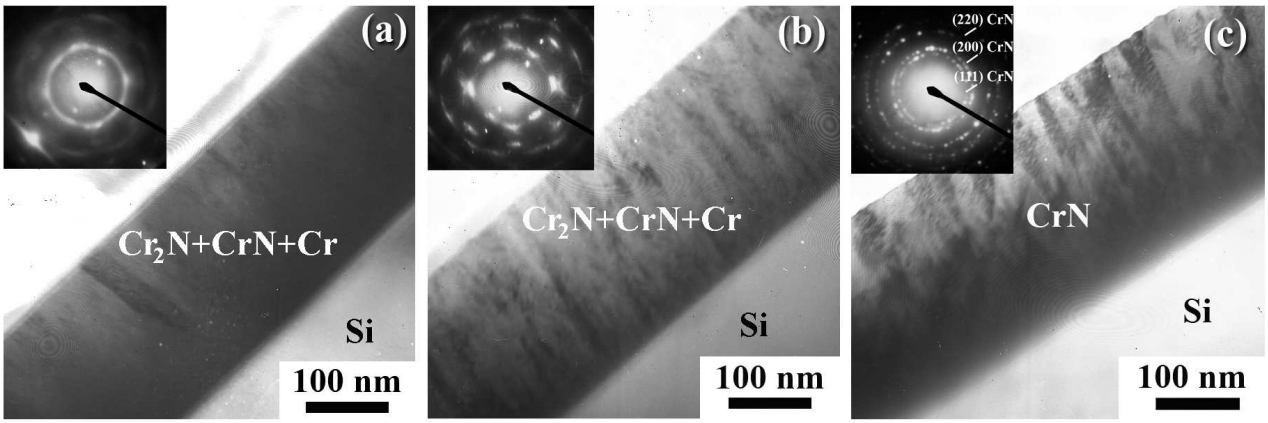

Figure 4. TEM images and corresponding MD patterns of Cr_xN_y thin films as a function of nitrogen partial pressure: a) 2×10^{-4} mbar, b) 3.5×10^{-4} mbar and c) 5×10^{-4} mbar

on different nitride thin films deposited by RF reactive magnetron sputtering. They revealed that a significant fraction of the Cr^+ ions exhibits a high flux and kinetic energy if the nitrogen partial pressure p_{N_2} is low. These high-energy ions effectively bombard the growing film and a densely packed morphology results. In contrast, in an absence of a significant amount of high-energy ions at higher p_{N_2}, the authors observed columnar crystal morphology.

3.2. Optical analyses

Optical properties of Cr_xN_y films were studied by SE (spectroscopic ellipsometry), which is non-destructive, surface-sensitive technique determining the complex dielectric function $\varepsilon(\omega)$ of the materials. Figure 5 shows the real (ε_r) and the imaginary (ε_i) parts of dielectric functions obtained from Cr_xN_y films deposited under different values of nitrogen partial pressure.

The dielectric functions of Cr_xN_y films were analysed through appropriate modelling, using the following points:

- One-layer model was used for each sample since these layers are optically thick.
- The pure Cr layer was modelled with Cr, while the other layers were modelled as a mixture of Cr, Cr_2N and CrN phases, by using the Bruggeman effective approximation. In BEMT any complex material is considered to consist of randomly mixed regions of pure constituent materials (Cr, Cr_2N, CrN); then, the dielectric function of complex material can be described by the dielectric functions of the constituent materials and the corresponding volume fractions.
- The dielectric function for the pure Cr layer was modelled using the Drude oscillator model, which is commonly used for metal systems and well describes metallic character due to the intraband transitions of free conduction electrons. The analysis of other samples was made by Drude term and Tauc-Lorentz oscillator (DTL model) described in literature [23], where Tauc-Lorentz model describes the interband transitions due to valence

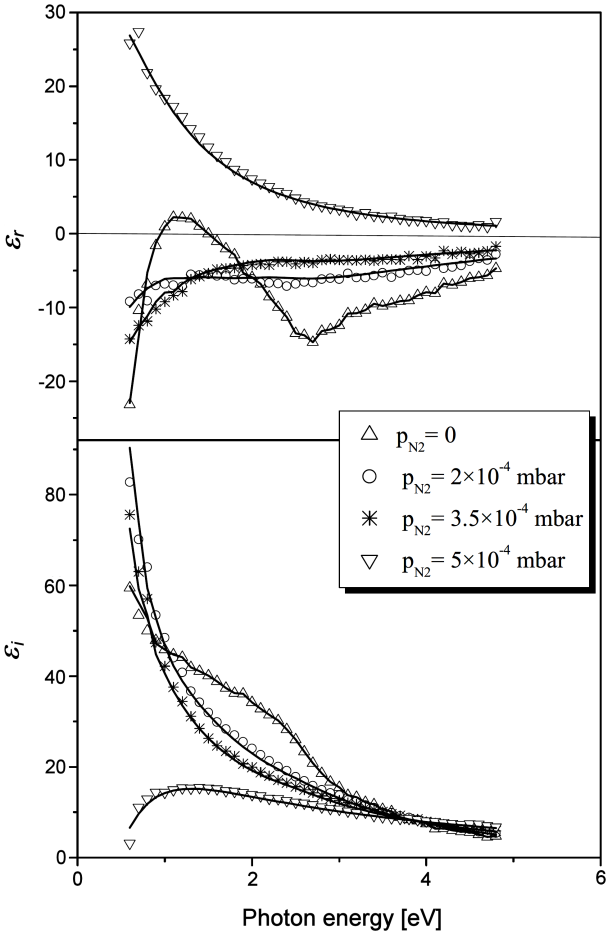

Figure 5. Real (ε_1) and imaginary (ε_2) part of the dielectric function of Cr_xN_y thin films deposited at different nitrogen partial pressures (continuous lines correspond to the fits obtained by models described in the text)

electrons. A special feature of materials with conduction electrons is the plasma frequency ω_p, which is correlated with the conduction electron density. Therefore, ω_p can be used to determine the metallic or semiconducting character of the Cr_xN_y films. Another important parameter is the damping factor Γ_D. This parameter is proportional to the collision frequency which can be related to the col-

lision processes between the free charge carriers and defects and hence give us information about the crystalline order in the system.

The fitting results of different Cr_xN_y films, obtained by using above mentioned modelling, are shown in Fig. 5. The volume fractions of different phases obtained by BEMT analysis are listed in Table 2. The four presented layers exhibit different composition, crystal structure and optical properties and correspond to Cr (p_{N_2} = 0 mbar), mixed Cr + Cr_2N + CrN (p_{N_2} = 2×10^{-4} and 3.5×10^{-4} mbar) and CrN (p_{N_2} = 5×10^{-4} mbar). According to the raw spectra, the pure Cr have $\varepsilon_r < 0$, indicating metallic character of the layer. Similar behaviour was observed for samples S-2 and S-3 deposited at nitrogen pressure of 2×10^{-4} and 3.5×10^{-4} mbar, respectively. On the other hand, the layer S-4 deposited at 5×10^{-4} mbar of nitrogen shows quite different behaviour having $\varepsilon_r > 0$. The results of the BEMT analysis show the variation of the constituent phases (Cr, Cr_2N and CrN) with the increase of nitrogen partial pressure. We identify three distinct regions where different phases dominate. For p_{N_2} = 0 there is no nitrogen incorporation in the layer and the pure Cr phase is formed. In the range of 2×10^{-4} mbar ≤ p_{N_2} ≤ 3.5×10^{-4} mbar primarily formed phase is Cr_2N, with different content of Cr and CrN. For p_{N_2} = 2×10^{-4} mbar the film consists of 70% of Cr_2N, 20% of Cr and 10% of CrN. When the nitrogen partial pressure is increased up to p_{N_2} = 3.5×10^{-4} mbar, Cr_2N becomes predominant phase in the layer with the volume fraction of 86%. Finally, for p_{N_2} = 5×10^{-4} mbar a pure CrN is formed. These results are in a good agreement with RBS and XRD findings.

Table 2. The volume fractions (f_i) of the constituent phases (Cr, Cr_2N, CrN) in various Cr_xN_y layers grown at different values of nitrogen partial pressure

Sample	S-1	S-2	S-3	S-4
p_{N_2} [mbar]	0	2	3.5	5
f_{Cr} [%]	100	21 ± 1	1 ± 1	-
f_{Cr_2N} [%]	-	69 ± 1	86 ± 1	-
f_{CrN} [%]	-	10 ± 1	13 ± 1	100

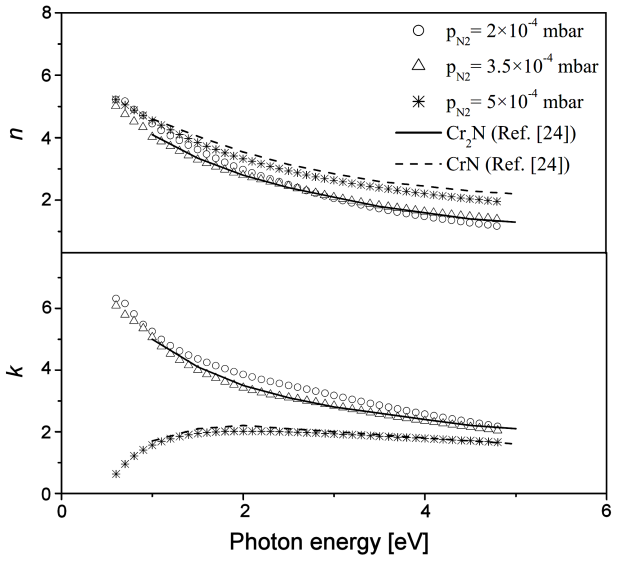

Figure 6. The calculated refractive index (n) and extinction coefficient (k) for Cr_xN_y thin films deposited at partial pressure of nitrogen of 2×10^{-4}, 3.5×10^{-4} and 5×10^{-4} mbar compared to the corresponding n, k curves for the pure CrN and Cr_2N [24]

Based on the results for the best-fit DTL parameters we calculated the refractive index n and extinction coefficient k in the energy region of 0.6–4.8 eV. Figure 6 shows the calculated n and k of the layer deposited at p_{N_2} = 5×10^{-4} mbar (the pure CrN) and the layers deposited at p_{N_2} = 2×10^{-4} and 3.5×10^{-4} mbar, containing predominantly Cr_2N phase. The solid and dashed lines represent the n, k values for the pure Cr_2N and CrN, respectively, reported by Aouadi *et al.* [24]. One can see that optical constants of our CrN layer quite well match with the one from the literature. Slightly smaller absolute values of refraction index in the whole energy range means that it is optically less dense as compared to the referent layer. As for the layers deposited at lower nitrogen partial pressures corresponding n and k versus photon energy shows different slopes, where the values for p_{N_2} = 3.5×10^{-4} mbar is in a good agreement with the literature values [24]. If one knows that these layers have different content of Cr_2N phase, namely 70% and 86% for p_{N_2} = 2×10^{-4} mbar and p_{N_2} = 3.5×10^{-4} mbar, respectively, it is concluded that even small change in the layer's composition influences its optical constants. Thus, establishing of an optical database for the Cr–N system enables us to easily identify different chromium-nitride phases (Cr_2N, CrN) and control their purity by monitoring the optical properties (based on SE data) of the layers.

The results of the DTL model fits can also determine the evolution of the transport properties of Cr_xN_y's conduction electrons. Figure 7 shows the ω_p and Γ_D values calculated from the Drude term of the DTL model. The discrimination of the various phases is obvious in the evolution of ω_p and Γ_D. In all cases Γ_D exhibits higher values with N incorporation as compared to the initial Cr layer. This parameter is closely related to the electrical resistivity and is influenced by the existence of grain boundaries and defects in the layers. Hence, the increase of Γ_D is attributed to the lower free electron mobility due to the structural differences in the layers. Indeed, there are some differences between our layers, not only compositional but also structural. As shown by TEM analysis (Fig. 4), by increasing the nitrogen partial pressure the average energy per atom of the growing film converts the compact stacking of the film (p_{N_2} = 2×10^{-4} mbar) over the less dense structure (p_{N_2} = 3.5×10^{-4} mbar) to the more porous, columnar structure (p_{N_2} = 5×10^{-4} mbar). Patsalas *et al.* [25] found that the Γ_D parameter is directly related to the content of voids in the layer and that Γ_D has the lowest value when the dense, compact structure is obtained, which is attributed to the elimination of voids.

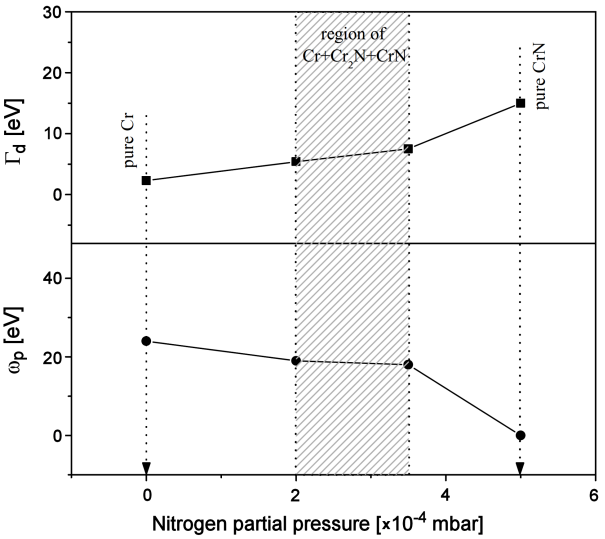

Figure 7. The evolution of ω_p and Γ_D calculated from the Drude term of the Drude and Drude-Tauc Lorentz model for different Cr_xN_y layers

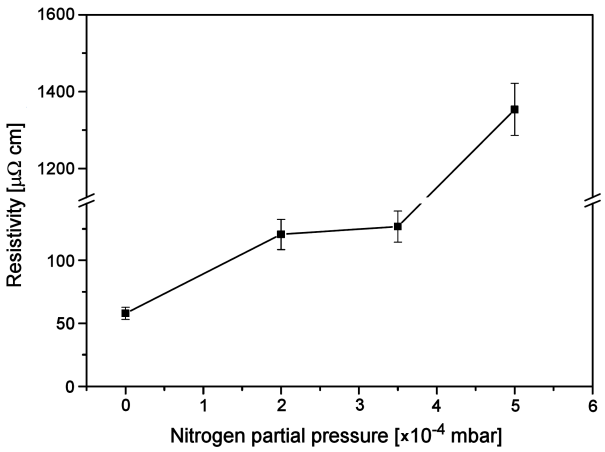

Figure 8. Variation of resistivity of Cr_xN_y layers as a function of nitrogen partial pressure during deposition

Figure 7 also shows an overall decrease of ω_p with increasing nitrogen content in the layers. Changes of ω_p could be directly related to the contribution of different phases and their metallic character. According to the results, Cr layer has pure metallic behaviour with the considerable density of conduction electrons (ω_p = 24 eV). In addition, with increasing nitrogen partial pressure to 2×10^{-4} mbar ω_p becomes lower and stays almost constant with further increase of p_{N_2} to 3.5×10^{-4} mbar. This is due to the incorporation of N into the layer, which is manifested in the formation of Cr_2N phase, with some contribution of Cr and CrN phases. For the nitrogen partial pressure of 5×10^{-4} mbar the layer exhibits no conduction electrons and consequently $\omega_p = 0$. This is an indication of semiconducting character of CrN, since at this p_{N_2} value a stoichiometric CrN phase is formed.

3.3. Electrical resistivity

The transport properties of Cr_xN_y's conduction electrons are better illustrated by the electrical resistivity measurements, based on the four point probe method. Figure 8 shows variation of resistivity of the Cr_xN_y films deposited under different nitrogen partial pressures. The resistivity of the pure Cr thin film corresponding to p_{N_2} = 0 mbar found to be about 58 μΩ cm, is in agreement with the value already reported by Högberg *et al.* [26]. When the nitrogen partial pressure is increased to 2×10^{-4} mbar (the sample S-2) the resistivity becomes more than two times higher than that of the Cr layer, reaching a value of 120 μΩ cm and stays almost constant when the nitrogen partial pressure is increased further up to 3.5×10^{-4} mbar (the sample S-3). The increasing trend of the electrical resistivity is due to the increase of N concentration in the layers which has as a consequence the increase of impurity defects or it may also be attributed to a decrease of the carrier density due to the nitrization of Cr. Based on the optical measurements (Table 2), combined by the XRD results (Fig. 2) the presence of different phases (Cr, Cr_2N and CrN) is established in the layers, with the primarily formed Cr_2N phase. Hence, electrical resistivity is higher as compared to the initial Cr film, but still metallic character is present in the layers [27]. By further increasing the nitrogen partial pressure to 5×10^{-4} mbar very high value of resistivity of 1353 μΩ cm is obtained. This clearly proves semiconducting character of CrN as only CrN phase grown under given nitrogen partial pressure. Similar findings were also reported by Subramanian *et al.* [28], who examined the influence of nitrogen flow rates on the properties of magnetron sputtered CrN_x films.

IV. Conclusions

The microstructure, optical and electrical properties of various Cr_xN_y films grown by DC reactive sputtering were studied. The layers were deposited at several values of nitrogen partial pressure ranging from 0 to 5×10^{-4} mbar. RBS and XRD were employed for the compositional analysis and phase identification. It was revealed that at different values of nitrogen partial pressure different phases are obtained: Cr (p_{N_2} = 0), mixed Cr + Cr_2N + CrN (p_{N_2} = 2×10^{-4} and 3.5×10^{-4} mbar) or pure CrN (p_{N_2} = 5×10^{-4} mbar). TEM has shown the changes in the morphology of the growing film: from compact and dense structure observed at p_{N_2} = 2×10^{-4} mbar to the well defined columnar structure for the highest nitrogen pressure. SE analysis was employed for the optical characterization of the samples. The results showed that there are well-defined p_{N_2} regions, where specific phases dominate (Cr, Cr_2N, CrN) and the optical constants n and k are directly determined by the presence of the growing phase. The layers with predominantly formed Cr_2N phase exhibit metallic behaviour, while CrN is a semiconductor.

Acknowledgements: This work was supported by the Ministry of Education and Science of the Republic of Serbia (Project No. III 45005). The authors are grateful

to D. Purschke for skillfully running the IONAS accelerator. Ion beam analysis of samples was done by Rutherford backscattering technique at the University in Göttingen.

References

1. B. Bushan, B.K. Gupta, *Handbook of Tribology*, McGraw-Hill, New York, 1991.
2. H.O. Pierson, *Handbook of Refractory Carbides and Nitrides - Properties, Characteristics, Processing and Applications*, Noyes Publications, Westwood, New York, 1996.
3. R.F. Bunshah, *Handbook of Hard Coatings: Deposition Technologies, Properties and Applications*, Noyes Publications, Norwich, New York, 2001.
4. Articles on Nitrides, Including: Boron Nitride, Beta Carbon Nitride, Gallium Nitride, Borazon, Aluminium Nitride, Nitride, Strontium Nitride, Titanium Nitride, Indium Nitride, Calcium Nitride, Lithium Nitride, Zirconium Nitride, Hephaestus Books, 2011.
5. R. Daniel, K.J. Martinschitz, J. Keckes, C. Mitterer, "Texture development in polycrystalline CrN coatings: the role of growth conditions and a Cr interlayer", *J. Phys. D: Appl. Phys.*, **42** (2009) 075401.
6. V.K. William Grips, V. Ezhil Selvi, H.C. Barshilia, K.S. Rajam, "Effect of electroless nickel interlayer on the electrochemical behavior of single layer CrN, TiN, TiAlN coatings and nanolayered TiAlN/CrN multilayer coatings prepared by reactive dc magnetron sputtering", *Electrochim. Acta*, **51** (2006) 3461–3468.
7. A.P. Ehiasarian, P.Eh. Hovsepian, L. Hultman, U. Helmersson, "Comparison of microstructure and mechanical properties of chromium nitride-based coatings deposited by high power impulse magnetron sputtering and by the combined steered cathodic arcyunbalanced magnetron technique", *Thin Solid Films*, **457** (2004) 270–277.
8. C. Constantin, M.B. Haider, D. Ingram, A.R. Smith, "Metal/semiconductor phase transition in chromium nitride(001) grown by rf-plasma-assisted molecular-beam epitaxy", *Appl. Phys. Lett.*, **85** (2004) 6371–6373.
9. D. Gall, C.S. Shin, R.T. Spila, M. Odén, M.J.H. Senna, J.E. Greene, I. Petrov, "Growth of single-crystal CrN on MgO(001): Effects of low-energy ion-irradiation on surface morphological evolution and physical properties", *J. Appl. Phys.*, **91** (2002) 3589–3597.
10. M.L. Kuruppu, G. Negrea, I.P. Ivanov, S.L. Rohde, "Monolithic and multilayer Cr/CrN, Cr/Cr_2N, and Cr_2N/CrN coatings on hard and soft substrates", *J. Vac. Sci. Technol. A*, **16** (1998) 1949–1955.
11. S. Logothetidis, P. Patsalas, K. Sarakinos, C. Charitidis, C. Metaxa, "The effect of crystal structure and morphology on the optical properties of chromium nitride thin films", *Surf. Coat.Technol.*, **180-181** (2004) 637–641.
12. G.A. Zhang, P.X. Yan, P. Wang, Y.M. Chen, J.Y. Zhang, "Influence of nitrogen content on the structural, electrical and mechanical properties of CrN_x thin films", *Mater. Sci. Eng. A*, **460-461** (2007) 301–305.
13. P. Patsalas, S. Logothetidis, "Interface properties and structural evolution of TiN/Si and TiN/GaN heterostructures", *J. Appl. Phys.*, **93** (2003) 989–998.
14. P. Patsalas, S. Logothetidis, "Optical, electronic, and transport properties of nanocrystalline titanium nitride thin films", *J. Appl. Phys.*, **90** (2001) 4725–4734.
15. F. Wooten, *Optical Properties of Solids*, Academic Press, New York, 1972.
16. M. Uhrmacher, K. Pampus, F.J. Bergmeister, D. Purschke, K.P. Lieb, "Energy calibration of the 500 kV heavy ion implanter ionas", *Nucl. Instrum. Methods B*, **9** (1985) 234–242.
17. N.P. Barradas, C. Jeynes, R.P. Webb, "Simulated annealing analysis of Rutherford Backscattering data", *Appl. Phys. Lett.*, **71** (1997) 291–293.
18. Horiba Scientific, DeltaPsi2 Software, Reference Manual, NP/DeltaPsi2R.Fm/264202–06/01/2010. Part No. 31 087 091.
19. M. Novaković, M. Popović, D. Peruško, V. Milinović, I. Radović, N. Bibić, M. Mitrić, M. Milosavljević, "Ion implantation induced structural changes in reactively sputtered Cr-N layers on Si substrates", *Nucl. Instrum. Meth. B*, **257** (2007) 782–785.
20. F.-H. Lu, H.-Y. Chen, "Phase changes of CrN films annealed at high temperature under controlled atmosphere", *Thin Solid Films*, **398-399** (2001) 368–373.
21. K.-W. Wang, T.-N. Lin, D.-Y. Wang, "Tribological property enhancement of CrN films by metal vapour vacuum arc implantation of vanadium and carbon ions", *Thin Solid Films*, **516** (2008) 1012–1019.
22. P. Hones, N. Martin, M. Regula, F. Lévy, "Structural and mechanical properties of chromium nitride, molybdenum nitride, and tungsten nitride thin films", *J. Phys. D: Appl. Phys.*, **36** (2003) 1023–1029.
23. M. Popović, M. Novaković, M. Mitrić, K. Zhang, N. Bibić, "Structural, optical and electrical properties of argon implanted TiN thin films", *Int. J. Refract. Met. Hard Mater.*, **48** (2015) 318–323.
24. S.M. Aouadi, D.M. Mihut, M.L. Kuruppu, S.R. Kirkpatrick, S.L. Rohde, "Spectroscopic ellipsometry measurements of chromium nitride coatings", *J. Vac. Sci. Technol. A*, **19** (2001) 2800–2804.
25. P. Patsalas C. Charitidis, S. Logothetidis, "In situ and real-time ellipsometry monitoring of submicron titanium nitride/titanium silicide electronic devices", *Appl. Surf. Sci.*, **154-155** (2000) 256–262.
26. H. Högberg, L. Tengdelius, M. Samuelsson, J. Jensen, L. Hultman, "Beta-Ta and alpha-Cr thin films deposited by high power impulse magnetron sputtering and direct current magnetron sputtering in hydrogen containing plasmas", *Physica B: Condensed Matter.*, **439** (2014) 3–8.
27. X.F. Duan, W.B. Mi, Z.B. Guo, H.L. Bai, "A comparative study of transport properties in polycrystalline and epitaxial chromium nitride films", *J. Appl. Phys.*, **113** (2013) 023701.
28. B. Subramanian, K. Prabakaran, M. Jayachandran, "Influence of nitrogen flow rates on materials properties of CrN_x films grown by reactive magnetron sputtering", *Bull. Mater. Sci.*, **35** (2012) 505–511.